

# A sweat-responsive covalent organic framework film for material-based liveness detection and sweat pore analysis

Received: 2 September 2022

Accepted: 25 January 2023

Published online: 03 February 2023

Check for updates

Qing Hao<sup>1</sup>✉, Xiao-Rui Ren<sup>2</sup>, Yichen Chen<sup>1</sup>, Chao Zhao<sup>1</sup>, Jingyi Xu<sup>1</sup>, Dong Wang<sup>2</sup>✉ & Hong Liu<sup>1</sup>✉

Covalent organic frameworks have shown considerable application potential and exceptional properties in the construction of stimulus-responsive materials. Here, we designed a sweat-responsive covalent organic framework film for material-based fingerprint liveness detection. When exposed to human sweat, the COF<sub>TPDA-TFPy</sub> film can transform from yellow to red. The COF<sub>TPDA-TFPy</sub> film, when touched by living fingers, can produce the naked-eye-identified fingerprint pattern through the sweat-induced color change, while artificial fake fingerprints cannot. This technique, which we named material-based liveness detection, can thus intuitively discern living fingers from fake fingerprints with a 100% accuracy rate. Additionally, the distribution of sweat pores on human skin can also be collected and analyzed by shortening the contact time. By merely washing them with ethanol, all the samples can be utilized again. This work inventively accomplished material-based liveness detection and naked-eye-identified sweat pore analysis and highlighted their potential for use in clinical research and personal identification.

Fingerprints are distinctive patterns that are personal to every individual. Fingerprints and their level 3 features, such as sweat pore distribution information<sup>1,2</sup>, are generally utilized as accurate standards in personal identification. Unfortunately, the existing personal identification systems based on fingerprints have often suffered attacks by artificial fake fingerprints, which pose serious hazards to individual safety and property<sup>3,4</sup>. Therefore, extensive effort has been put into developing fingerprint identification systems that can distinguish between living fingers and fake fingerprints, which are defined as liveness detection<sup>3,4</sup>. Previously, fingerprint liveness detections were generally accomplished by extracting and analyzing the patterns and level 3 features of the fingerprint images of living fingers and fake fingerprints based on sophisticated computer algorithms in the field of computer science<sup>5-9</sup>. From the perspective of material science, it is quite appealing to develop a type of material that could simply

distinguish living fingers from fake fingerprints at the time of fingerprint collection. In this case, liveness detection would be achieved through the design of fingerprint collection materials, rather than computer software development. Realizing the liveness detection based on material science, which we defined as material-based liveness detection, may offer a practical solution to the computer science problem through a material strategy.

One of the biggest differences between fake fingerprints and living fingers is that fake fingerprints cannot secrete sweat like living fingers. Using sweat-responsive materials instead of optical sensors to collect sweat fingerprints should be possible to naturally discern between living fingers and fake fingerprints. Here, we divide the fingerprint matching process into two steps: the fingerprint collection step and the fingerprint recognition step (Fig. 1a). The previous code-based fingerprint liveness detection method occurred in the

<sup>1</sup>State Key Laboratory of Bioelectronics, School of Biological Science and Medical Engineering, Southeast University, 2# Sipailou, Nanjing, Jiangsu 210096, China. <sup>2</sup>Key Laboratory of Molecular Nanostructure and Nanotechnology, Beijing National Laboratory for Molecular Sciences, CAS Research/Education Center for Excellence in Molecular Sciences, Institute of Chemistry, Chinese Academy of Sciences, Beijing 100190, P.R. China. ✉e-mail: [haocq@seu.edu.cn](mailto:haocq@seu.edu.cn); [wangd@iccas.ac.cn](mailto:wangd@iccas.ac.cn); [liuh@seu.edu.cn](mailto:liuh@seu.edu.cn)

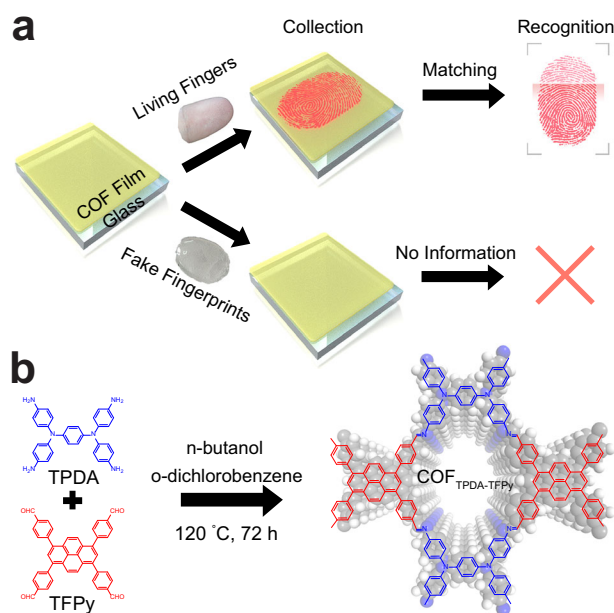


**Fig. 1 | Material-based liveness detection with COF film.** **a** Schematic of the material-based liveness detection based on the COF<sub>TPDA-TFPy</sub> film. **b** Chemical structures of monomers and COF<sub>TPDA-TFPy</sub>.

recognition step by image processing<sup>5–9</sup>, whereas the material-based liveness detection approach would discriminate at the fingerprint collection stage. However, there is still no research on material-based liveness detection methods till now. We believe that developing a type of sweat-responsive material, that can produce naked-eye-identified fingerprints and their level 3 feature patterns, would be a good substitute for fingerprint collection. In this situation, living fingers would generate fingerprint images on the sweat-responsive material, whereas fake fingerprints cannot supply any information, enabling the material-based liveness detection to be realized.

Covalent organic frameworks (COFs) are a class of porous organic polymers with stable chemical properties and long-range ordered crystal structures that have experienced explosive development over the past decade<sup>10–17</sup>. The designable chemical composition and structure confer COFs a variety of functions, and COFs have been successfully applied in the fields of gas storage and separation<sup>18–21</sup>, catalytic science<sup>22–24</sup>, chemical sensing<sup>25–27</sup>, energy science and electrochemistry<sup>28–33</sup>. Among them, stimulus-responsive chromogenic COFs, including solvatochromic<sup>34–36</sup>, acidochromic<sup>37–39</sup>, and electrochromic COFs<sup>40–43</sup>, have aroused growing research interest. These works highlighted the critical contribution of COFs' highly ordered porous crystal structures to the improvement of stimulus-response properties. For instance, the highly ordered COFs exhibit solvatochromic phenomena much better than commercial materials, with an ultra-fast response time and great reversibility<sup>34</sup>. We believe that the functional COF materials with a long-range ordered pore structure would show effective color change to water, organic acids, or other compositions in sweat, and achieve reusable and instrument-free fingerprint collection and analysis for material-based liveness detection.

In this work, we have achieved material-based fingerprint liveness detection based on COF film. The sweat-responsive COF<sub>TPDA-TFPy</sub> film with good crystallinity was directly grown on the transparent glass substrates (Fig. 1b). When subjected to humidity streams, COF<sub>TPDA-TFPy</sub> film can alter its color from yellow to red in a reversible manner, whereas sweat leaves a stable color change that does not naturally fade. After being gently touched by a human finger for around 10 s, the trace sweat secreted by sweat pores in the friction ridge caused a steady color change in the contact area of the COF<sub>TPDA-TFPy</sub> film.

Then, a naked-eye-identified sweat-induced fingerprint was left on the COF<sub>TPDA-TFPy</sub> film, while the fake fingerprints left no imprint (Fig. 1a). Sweat-induced fingerprints from the same donor can be easily matched in the database by fingerprint matching software, and 100% of the attacks of fake fingerprints can be blocked before the recognition step. Therefore, material-based liveness detection was naturally realized with a 100% accuracy rate in the sight of material science. Additionally, by reducing the contact time (for around 1–5 s), the sweat pore distribution information from fingerprints and other parts of the body can also be gathered. Since many diseases (such as dermatosis and endocrinosis) may be associated with sweat secretion behavior, this sensitive analysis method may provide information on the distribution and sweat secretion behavior of sweat pores, and thus may provide a perspective for clinical research in the future. All of these samples can be quickly and easily collected, evaluated, and reused more than 50 times by washing with ethanol without the need for large instruments. We believe that this work would provide a unique sight to the field of personal identification based on material science and would have a broad range of potential applications.

## Results and discussion

### Preparation and characterization of COF<sub>TPDA-TFPy</sub> powders and films

Typically, the COF<sub>TPDA-TFPy</sub> powders were synthesized through the solvothermal method at 120 °C for 72 h, taking the o-dichlorobenzene (o-DCB) and n-butanol (n-BuOH) mixture as solvent. N, N, N', N'-tetraakis(4-aminophenyl)-1,4-benzenediamine (TPDA) and 1,3,6,8-Tetrakis(4-formylphenyl)pyrene (TFPy) were chosen as building blocks, and 6 M acetic acid (HOAc) aqueous as catalyst (Fig. 1b). A number of strong reflections were observed in the powder X-ray diffraction (PXRD) pattern of COF<sub>TPDA-TFPy</sub> powders at 5.41° (110), 7.59° (200), 10.81° (220), 12.0° (310), and 20.9° (001). Following Pawley refinement, the P2/m symmetric structural model of COF<sub>TPDA-TFPy</sub> offers well fit for these experimental results. The unit cell parameters were calculated as a = 2.35 nm, b = 2.28 nm, c = 0.43 nm, α = β = 90°, γ = 78°, respectively (Supplementary Figs. 1, 2; Table 3). Meanwhile, Fourier-transform infrared spectroscopy (FTIR) and <sup>13</sup>C nuclear magnetic resonance (NMR) spectra of COF<sub>TPDA-TFPy</sub> were also measured. The peak in the FTIR spectra of COF<sub>TPDA-TFPy</sub> at around 1630 cm<sup>-1</sup> revealed the stretching mode of the imine bonds (-C=N). At the same time, the decreasing of peaks at around 1690 cm<sup>-1</sup> (characteristic peak of the -CHO groups) and around 3200 cm<sup>-1</sup> (characteristic peaks of the Ph-NH<sub>2</sub> groups) further confirmed the occurrence of the Schiff bases reactions (Supplementary Fig. 3). Additionally, the chemical shift at roughly 153 ppm (carbon g) in the <sup>13</sup>C NMR spectra strongly corroborated the successful synthesis of imine bonds, while all the other carbon resonances can be assigned to the chemical structure of COF<sub>TPDA-TFPy</sub> (Supplementary Fig. 4). The Brunauer–Emmett–Teller (BET) experiment data showed a nitrogen adsorption Type-I isotherm with a sharp step at P/P<sub>0</sub> < 0.01, which supports the micropore structure of COF<sub>TPDA-TFPy</sub> (Supplementary Fig. 5a)<sup>44</sup>. The pore size distribution (PSD) profiles obtained using non-local density functional theory revealed a very narrow pore size distribution with a maximum at 1.32 nm, which fit well with the atomistic model of COF<sub>TPDA-TFPy</sub> (Supplementary Fig. 5b). These results demonstrated that COF<sub>TPDA-TFPy</sub> powders were successfully prepared.

To facilitate subsequent study, the COF<sub>TPDA-TFPy</sub> films were also directly grown on the transparent glass using the solvothermal method (See “Methods” section). The as-prepared COF<sub>TPDA-TFPy</sub> films displayed a consistent yellow morphology (Fig. 2a). The images of scanning electron microscopy (SEM) and atomic force microscopy (AFM) revealed that the COF<sub>TPDA-TFPy</sub> film was formed by the stacking of small quadrilateral nanosheets with a thickness of around 100 nm (Supplementary Figs. 6, 7). The transmission electron microscopy (TEM) images were collected by scraping the film from the substrate.

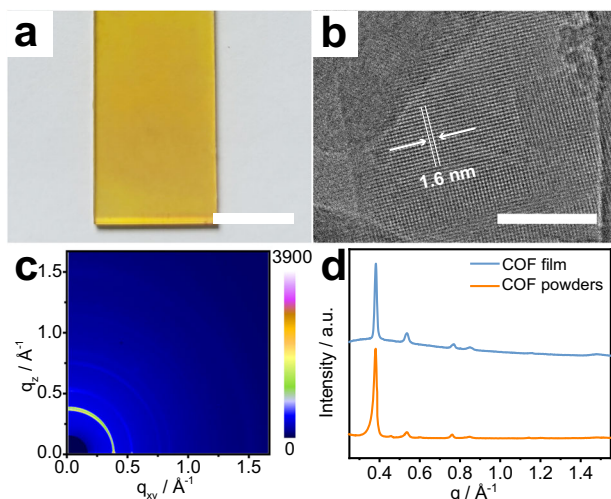


**Fig. 2 | Characterization of COF<sub>TPDA-TFPy</sub> film.** **a** Photograph of COF<sub>TPDA-TFPy</sub> film. (Scale bar: 1 cm) **b** TEM images of COF<sub>TPDA-TFPy</sub> film. (Scale bar: 50 nm) **c** GIWAXS data of the COF<sub>TPDA-TFPy</sub> film on glass substrates. **d** Projections of GIWAXS data of COF<sub>TPDA-TFPy</sub> films near  $q_z = 0$  (Blue) and PXRD data of COF<sub>TPDA-TFPy</sub> powder (Orange).

As shown in Fig. 2b, the vast area of periodic pore pattern was observed on the COF<sub>TPDA-TFPy</sub> nanosheets. The pore structure is consistent well with the predicted structure of COF<sub>TPDA-TFPy</sub> and showed a pore-to-pore period of around 1.6 nm. (Supplementary Figs. 8, 9). Meanwhile, the 2D synchrotron radiation grazing incidence wide-angle X-ray scattering (GIWAXS) data of COF<sub>TPDA-TFPy</sub> film was also recorded. The Bragg peaks appeared as diffraction rings (Fig. 2c), and the projections of the data sets near  $q_z = 0$  gave the diffraction peaks at 0.38 (110), 0.54 (200), 0.77 (220), 0.85 (310), and 1.48 Å<sup>-1</sup> (001), which could agree well with the PXRD of COF<sub>TPDA-TFPy</sub> powders (Fig. 2d). These results verified the successful synthesis of the COF<sub>TPDA-TFPy</sub> film.

### Material-based liveness detection of fingerprints

Touching the COF<sub>TPDA-TFPy</sub> film with a living finger for 10 s would result in a naked-eye-identified dark-red fingerprint impression on the yellow film (Fig. 3a, b; Supplementary Movie 1). At first, we believed this phenomenon can be attributed to the hydrochromism of COF. Actually, the COF<sub>TPDA-TFPy</sub> films do exhibit remarkable hydrochromic phenomena. As shown in Fig. 3c, exposing the COF<sub>TPDA-TFPy</sub> film to humidity N<sub>2</sub> stream results in a color change from yellow to red. The humidity breathing also showed a similar phenomenon (Supplementary Movie 2). However, the color change of COF<sub>TPDA-TFPy</sub> film caused by water is totally reversible after drying, while the sweat-resulted pattern would not disappear naturally. Therefore, although the color change is similar, we believe that the sweat-induced color change

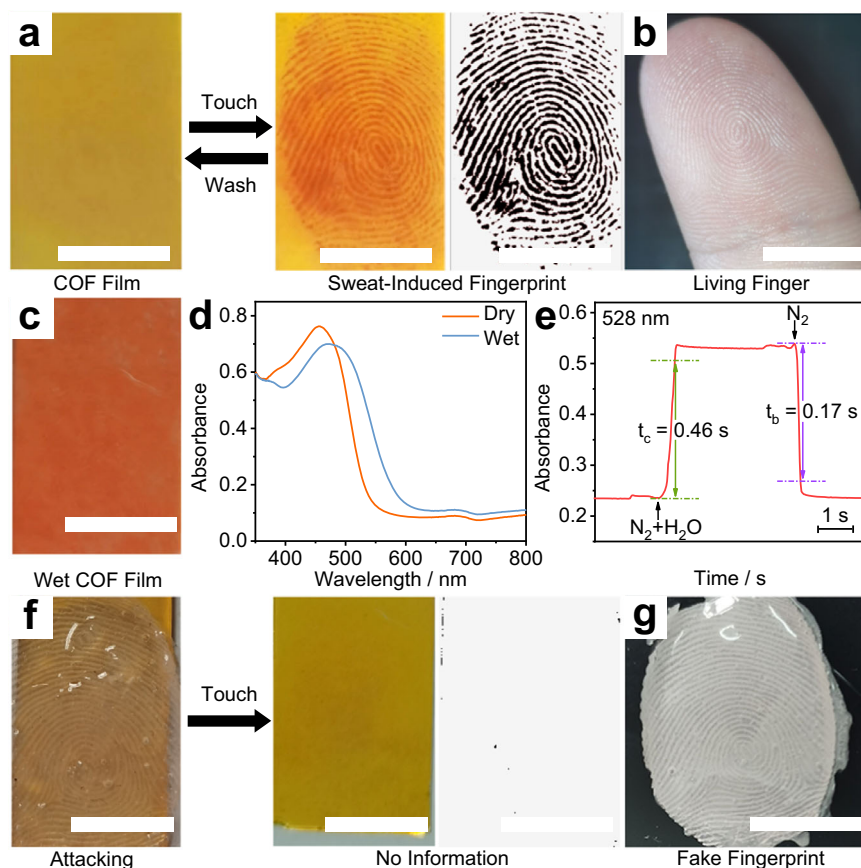


**Fig. 3 | Sweat-induced fingerprint collected by COF<sub>TPDA-TFPy</sub> film.** **a** Photograph of COF<sub>TPDA-TFPy</sub> film before and after the touch of human fingers for 10 s taken by a smartphone. The image with grey background is the sweat-induced fingerprint extracted using Photoshop. The black colored images are added pseudocolors by a Photoshop program for clear display. **b** Photographs of a living finger. **c** Photographs of COF<sub>TPDA-TFPy</sub> film at wet (N<sub>2</sub> + H<sub>2</sub>O) condition. **d** Corresponding

absorption spectra at dry and wet conditions, respectively. **e** Response time of COF<sub>TPDA-TFPy</sub> film at 528 nm by alternately exposing the COF<sub>TPDA-TFPy</sub> film to wet and dry N<sub>2</sub> stream. **f** Photographs of COF<sub>TPDA-TFPy</sub> film attacked by artificial fake fingerprint. **g** Corresponding artificial fake fingerprint from the finger in (b). (Scale bars: 1 cm).

comes from both water and other complex components of sweat, rather than simple hydrochromism.

We then experimented with several typical sweat compositions. With humidity stream stimulation for the water initially, the absorbance peak of COF<sub>TPDA-TFPy</sub> film, which was previously at about 457 nm in the absorption spectra, migrated to about 480 nm (Fig. 3d). The previous work<sup>34</sup> suggested that solvent-induced electronic structure change is responsible for the solvatochromic characteristics of COFs. The hydrochromic features brought on by electronic processes would be encouraged by the periodic donor-acceptor pairings in the COF skeleton. Consequently, the COF<sub>TPDA-TFPy</sub> film containing intramolecular donor-acceptor pairs resulted in a pronounced electronic structure-based hydrochromic phenomenon (Supplementary Fig. 10). The absorbance value at 528 nm, the wavelength displayed the highest variation (Supplementary Fig. 11), switched quickly as the N<sub>2</sub> stream alternated between the dry and humid states (Fig. 3e). The ultra-fast coloring time ( $t_c$ ) and bleaching time ( $t_b$ ) at 528 nm, where the absorbance value changed by more than 90%, were estimated as 0.46 s and 0.17 s, respectively. Meanwhile, within 50 switching cycles, the absorbance value kept switching steadily (Supplementary Fig. 12). Even if there are minor changes in the absorption spectra after 200 cycles, it can essentially return to its previous state after being washed with ethanol (Supplementary Fig. 13).

For other components, the COF<sub>TPDA-TFPy</sub> film was treated by solutions with some common ingredients in sweat. Some acids can produce a grey tint, which may be caused by COF protonation. (Supplementary Table 1). And some compositions like some protein (e.g. dermcidin, one of the most abundant proteins in sweat<sup>45</sup>) solutions could generate a stable red area (Supplementary Fig. 14; Table 1). We supposed that the moisture in proteins from the sweat and the water-holding capacity of these proteins may provide a stable humidity

micro-environment in the fingerprint residue<sup>46,47</sup> left on the COF<sub>TPDA-TFPy</sub> film. After contact, the FTIR spectrum of the COF<sub>TPDA-TFPy</sub> pellet showed rising -OH bands, which also supported the presence of water residue (Supplementary Fig. 15). Considering that the color and spectral changes caused by sweat are similar to those caused by water, we speculate that the synergistic interaction of these components in sweat resulted in the long-term sweat-responsive deep red color.

Washing with ethanol is a straightforward method for erasing these stable images (Fig. 3a). Despite some unavoidable wear and tear, after 50 cycles of touch-and-wash operations, the COF<sub>TPDA-TFPy</sub> film can still provide clear enough images (Supplementary Fig. 16). The good reusable ability makes the per-collection cost less than 0.02 dollars.

Note that such sweat-induced fingerprints can only be derived from the sweat secretion of living fingers, the artificial fake fingerprint (Supplementary Fig. 17) that cannot secrete sweat did not generate any imprints (Fig. 3f, g). However, the artificial fingerprint can mimic a living finger to generate a realistic-looking fingerprint with colored inks (Supplementary Fig. 18), which can pose a great threat to personal safety and personal property safety. Therefore, the COF<sub>TPDA-TFPy</sub> film can simply and directly collect sweat-induced fingerprints, and at the same time distinguish between living fingers and fake fingerprints. As we proposed above, the COF-based fingerprint collection and recognition method can be defined as material-based liveness detection. In this scenario, fake fingerprint attacks are unable to produce any meaningful patterns and can therefore be blocked as early as the collection step rather than the following recognition step.

The fingerprint patterns collected by COF<sub>TPDA-TFPy</sub> film were highly compatible with the existing fingerprint recognition software. We use a simple approach fingerprint matching code created by V. K. Alilou<sup>48</sup> to test fingerprint recognition and the accuracy of material-based liveness detection. As shown in Fig. 4, the minute details in the

**Table 1 | Similarity factors of 12 fingerprint samples from one donor with the fingerprint sample in Fig. 4a**

Sample	Similarity factor	Sample	Similarity factor	Sample	Similarity factor
101_1	0.78791	101_5	0.73	102_1	1
101_2	0.85896	101_6	0.74726	102_2	0.81111
101_3	0.81698	101_7	0.69437	102_3	0.84327
101_4	0.86518	101_8	0.80556	102_4	0.76422

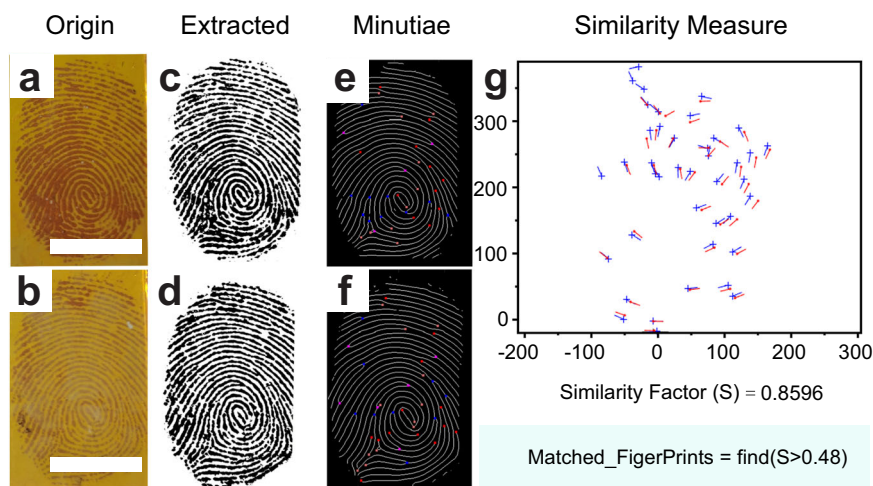


**Fig. 4 | Sweat-induced fingerprint recognition step. a, b** Photographs of two sweat-induced fingerprints. **c, d** Images extracted from (a, b), respectively. The black (c, d) colored images are added pseudocolors by a Photoshop program for

clear display. **e, f** Minutiae images calculated from (c, d). **g** The result of the similarity measure with a similarity factor of 0.8596 (Scale bars: 1 cm).

two fingerprint samples from the same donor are identical, and the similarity factor was calculated to be 0.8596 ( $>0.48$  would be used to confirm that the samples are from the same person). At the same time, the fake fingerprint left no information on the film and the software was inoperable.

Another 12 fingerprint samples (Number 101\_1 - 102\_4) collected by COF<sub>TPDA-TFPy</sub> film from the same donor (Supplementary Data 1) have also been added to the database with a total fingerprint sample of 72 (From FVC2002<sup>49</sup>, number 102\_5 - 109\_8). The 12 fingerprints belonging to the same donor can be fully identified through database comparison (Table 1), and the 60 other fingerprint samples can also be fully discriminated (Supplementary Table 2). At the same time, none of the fake fingerprint attacks had any meaningful outcomes. This indicated that the material-based liveness detection method can completely block the fake fingerprint at the collection step time, which provides a totally different solution notion from that of computer science<sup>3-9</sup>. In contrast to the computer science method, in which the liveness detection steps are carried out after the image collection step, this material-based liveness detection occurs as early as the collection step rather than the subsequent recognition step. Be aware that fake fingerprints cannot produce useful information and do not require the subsequent fingerprint-matching procedure. Here, material-based liveness detection can be accomplished in a straightforward manner and from the perspective of material science.

### Sweat pore analysis

In addition, reducing the contact time to around 1 s with human fingers can generate a red color dot pattern that matches the sweat pores on the finger (Fig. 5a, b; Supplementary Movie 3). The sweat pore information is one of the level 3 features of fingerprints, which would be

valuable for personal identification based on normal or partial fingerprints<sup>12</sup>. Moreover, the detection of active sweat pores is another liveness detection method in computer science<sup>3-9</sup>. The sweat pores images on COF<sub>TPDA-TFPy</sub> film can be directly identified by the naked eye, and easily collected just by taking photos with smartphones and using Photoshop to extract and analyze the pattern conveniently. This is different from the previous sweat pore collection methods based on solvatochromic fluorescence<sup>50-53</sup>, mass spectrometry<sup>54</sup>, electrochemiluminescences<sup>55</sup>, and scanning electrochemical microscopy<sup>56</sup> that need the help of additional instruments. For ordinary persons without prior instrument operation experience, the instrument-free method makes data gathering and processing convenient. Moreover, the sweat pore distribution images generated by COF<sub>TPDA-TFPy</sub> film can also be considered as a material-based liveness detection feature to avoid attacks of fake fingerprints in the future.

Three different fingerprints were taken on three COF<sub>TPDA-TFPy</sub> films in order to assess the reproducibility of the COF-based sweat pore distribution imaging approach (Fig. 5a, b; Supplementary Fig. 19). The sweat pore images of the three samples were extracted and superimposed (Added pseudocolors). As shown in Fig. 5c, the three samples are in good agreement. The precise identification and location of non-active sweat pores can also be accomplished by superimposing the active sweat pore distribution images on the fingerprint obtained using graphite. As shown in Fig. 5d, the green circles display the non-active sweat pores that did not secrete sweat.

In addition to the hairless finger, we also attempted to collect data on the distribution of sweat pores from other body areas, such as the instep, the inside of the arm with imperceptible villi, and the hairy outside of the arm (Fig. 5e, f; Supplementary Fig. 20). On the instep and the inner side of the arm, the irregularly dispersed sweat pore patterns

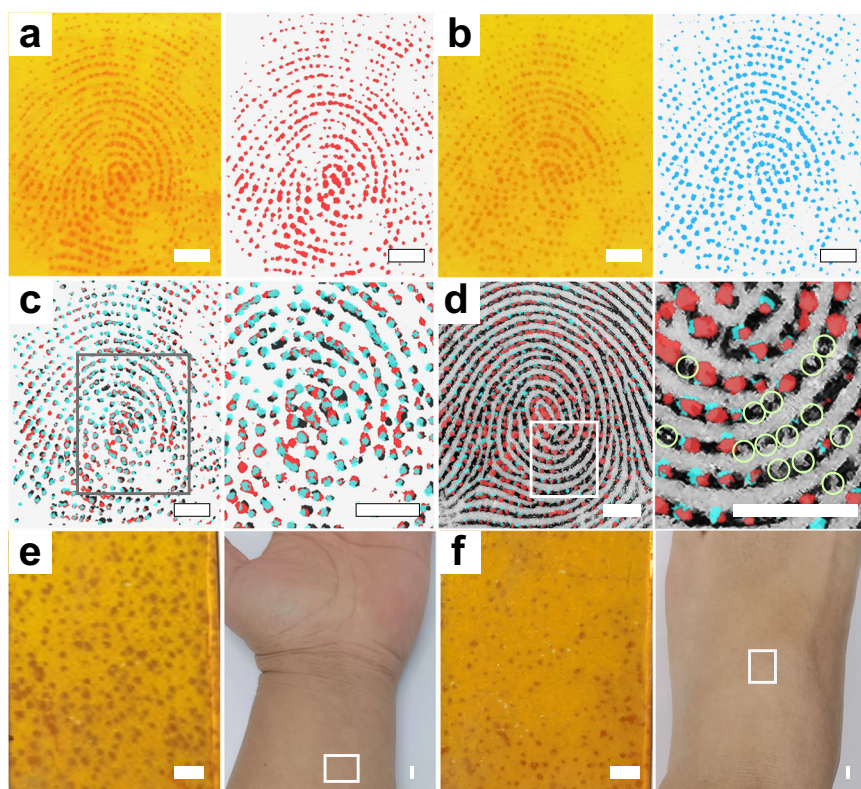


**Fig. 5 | Sweat pore images collected by COF<sub>TPDA-TFPy</sub> films. a, b** Picture of 2 independent sweat pore distribution images and extracted sweat pore distribution images on 2 individual COF<sub>TPDA-TFPy</sub> films from the same donor (Taken with a smartphone) c Superimposed images of 3 sweat pore images. d Superimposed image of sweat pore distribution images on a graphite fingerprint image. The green

circles showed the non-active sweat pores. e Sweat pore distribution images collected from the inside of the arm. f Sweat pore distribution images collected from the instep (Scale bars: 20 mm). The red (a, c, d), blue (b, c, d), and black (c) colored images are added pseudocolors by a Photoshop program for comparison purposes.

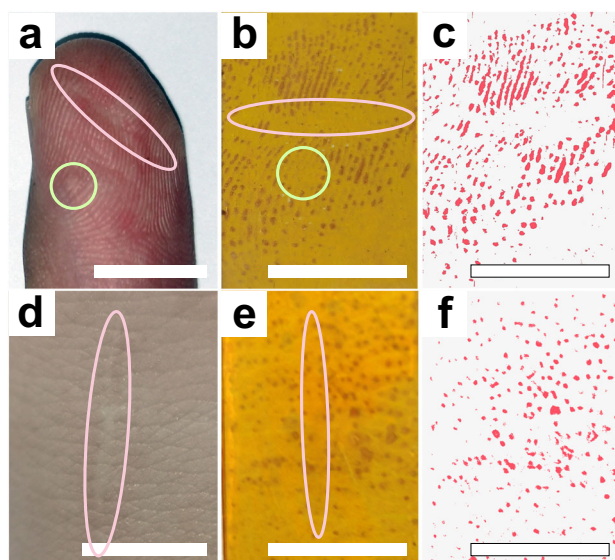


**Fig. 6 | Sweat pore images of scars and keratosis.** **a** Photograph of a finger with scars (red circle) and mild keratosis (green circle). **b** Sweat pore images collected from the finger in (a). **c** Extracted sweat pore images from (b). **d** Photograph of an area of the inside of an arm with scars (red circle) **e** Sweat pore images collected from the area in (d). **f** Extracted sweat pore images from (e). (Scale bars are 1 cm) The red (c, f) colored images are added pseudocolors by a Photoshop program for clear display.

can be directly collected (Fig. 5e, f). When collecting the hairy outside of the arm, the hair sometimes affects image acquisition (Supplementary Fig. 20b). But following shaving, similar sweat pore distribution patterns can be gathered on the hairy arm's outer skin surface. (Supplementary Fig. 20c). In contrast to the fingers, which have friction ridges, other body parts have an irregular distribution of sweat pores. Therefore, even after prolonged contact (>10 s), the sweat pores photos will still show a scattered dot pattern rather than lines like fingerprints.

This simple and rapid strategy for visualization and localization of sweat pores may have potential value in physiological and pathological studies. For example, a contributor had both scars and mild keratosis on his fingers (Fig. 6a). The image collected by COF films revealed that the center of the healed scar still lacks the ability for sweat pores to operate normally. Additionally, even while active sweat pores can be seen on keratinized skin, these pores have much lower sweat secretion capacities than the sweat pores around them, which may be a marker of local lesions or one of their causes (Fig. 6b, c). We also discovered that the sweat pores in the center of the scar on the arm did not regenerate even after healing, similar to what was seen on the fingers (Fig. 6d–f). Given that many diseases result in abnormal sweating, information about the distribution and ratio of active versus inactive sweat pores may act as useful supporting data for clinical research in the future.

In summary, we have demonstrated fingerprint material-based liveness detection based on a sweat-responsive COF film. The COF<sub>TPDA-TFPy</sub> film exhibited good crystallinity and reversible hydrochromic phenomena between yellow and red, and sweat can produce a long-term color change. Living fingers touching the COF<sub>TPDA-TFPy</sub> film for 10 s can generate naked-eye-identified sweat-induced fingerprints, whereas the artificial fake fingerprints cannot provide meaningful images. Therefore, while collecting fingerprint images, the COF<sub>TPDA-TFPy</sub> film can naturally distinguish living fingers from fake fingerprints. Simply taking photos with smartphones can capture all of the fingerprint images, which can then be examined by fingerprint-matching software. This method is capable of 100% fingerprint recognition and

100% fake fingerprint identification in the way of material science, and we defined it as material-based liveness detection. By washing with ethanol, repeated collections can be made more than 50 times. Additionally, the sweat pore distribution images of human skin can also be collected. This method may also be used to study sweating behavior and pathological alterations to the skin's surface. In the future, we will continue to encourage the use of this COF film-based analytic technique in the fields of clinical medical research and safe personal identification.

## Methods

### Materials and chemicals

The monomers, N, N, N', N'-tetrakis(4-aminophenyl)-1,4-benzenediamine (TPDA, 95%) and 1,3,6,8-Tetrakis(4-formylphenyl)pyrene (TFPy, 95%) were supplied by Chemsoon Co., Ltd. Acetic acid (HOAc, 99.5%) was bought from TCI Co., Ltd. Solvents including 1,2-dichlorobenzene (o-DCB, 99 + %), 1-Butanol (n-BuOH, 99.5%) and dimethylformamide (DMF, 99.5%) were bought from Acros Organics Co., Ltd. Normal solvents like tetrahydrofuran (THF, AR) and ethanol (AR) were bought from Nanjing Chemical Reagent Co., Ltd. (Nanjing), and Aladin Co., Ltd. Ultrapure water ( $\geq 18$  M $\Omega$ , Milli-Q, Millipore) was used throughout the experiment. All chemicals were used without further purification.

### Preparation of COF<sub>TPDA-TFPy</sub> powders

Typically, the TPDA (47.3 mg, 0.10 mmol) and TFPy (61.8 mg, 0.10 mmol) were charged in a high vacuum thick wall reaction bottle (15 mL of volume,  $\phi_{in} = 2.0$  cm), the 1,2-dichlorobenzene (3 mL) and 1-butanol (3 mL) were added as mixture solvent. Then, 0.4 mL of 6 M HOAc was added to the solution and the mixture was sonicated for 30 minutes. After a traditional degassing process with three freeze-pump-thaw cycles, the reaction bottle was sealed off and left until room temperature. The sealed reaction bottle was subsequently heated and kept at 120 °C for 72 h. The resulting precipitates were collected by filtration and washed with water, DMF, and THF 3 times each. Then, COF<sub>TPDA-TFPy</sub> powders were further activated by Soxhlet extraction with tetrahydrofuran for 12 h. Finally, the COF<sub>TPDA-TFPy</sub> powders were dried under vacuum at 70 °C for 24 h.

### Preparation of COF<sub>TPDA-TFPy</sub> film

For the preparation of COF<sub>TPDA-TFPy</sub> film, the process is the same as that for the synthesis of COF<sub>TPDA-TFPy</sub> powders, except that the TPDA and TFPy were reduced to 14.2 mg (0.03 mmol) and 18.6 mg (0.03 mmol), respectively. Transparent glass substrates were cut into 1.5 cm  $\times$  4.5 cm and immersed into the mixture in the reaction bottle vertically. The resulting COF<sub>TPDA-TFPy</sub> films were rinsed with DMF and THF 3 times each and immersed in 75% ethanol before investigation.

### Absorption spectra measurements

In-situ absorption spectra were monitored by an Agilent Technologies Cary 60 UV-Vis spectrophotometer. For the hydrochromic investigation operation, a COF<sub>TPDA-TFPy</sub> film on the glass substrate was directly put in a quartz cuvette, and a gas tube ( $\phi_{in} = 0.8$  cm) of a home-build gas flow control system was put on the COF<sub>TPDA-TFPy</sub> film. In the two gas paths in the control system, the dry N<sub>2</sub> can directly pass or through the gas washing bottle with water, respectively. The switching of the dry/wet N<sub>2</sub> stream is realized by switching the gas path valve in the system.

### Fingerprints and sweat pores collection

The COF<sub>TPDA-TFPy</sub> films are taken from the 75% ethanol and put in a box with silica-gel driers to make sure they exhibited a yellow appearance. The human fingers were first cleaned with 75% ethanol wipes and then fully dried with a tissue. Fingerprints were collected by softly touching on the COF<sub>TPDA-TFPy</sub> film using living fingers for -10 s and sweat pore images were collected from fingers or other parts of the body for 1-5 s respectively. The as-collected samples can be identified directly by the

naked eye and obtained by taking pictures using a smartphone (Honor V30). The exact fingerprint images and distribution information of sweat pores can be extracted by Photoshop and added pseudo colors.

### Inclusion & ethics

All experiments were carried out in strict compliance with the relevant laws and with the approval of the Scientific Ethical Committee of the School of Biological Sciences and Medical Engineering, Southeast University. All the human research participants have signed a consent form.

### General characterization

PXRD patterns were collected by a PANalytical Empyrean Diffractometer with Cu K $\alpha$  radiation ( $\lambda = 1.5416 \text{ \AA}$ ) ranging from  $3.5^\circ$  to  $35^\circ$  with a speed of  $1^\circ/\text{min}$  at ambient temperature operated at 40 kV and 40 mA. The morphology of COF<sub>TPDA-TFPy</sub> film was studied by Scanning Electron Microscope (Zeiss Ultra Plus Field Emission Scanning Electron Microscope) and Atomic Force Microscope (Bruker Multimode 8). Themis 300 was employed to obtain the Transmission Electron Microscopy images using low-dose techniques at an accelerating voltage of 300 kV. Fourier transform infrared spectroscopy (FTIR) spectra were collected by a Thermo Scientific Nicolet 5700 instrument.  $^{13}\text{C}$  cross-polarization magic angle spinning nuclear magnetic resonance ( $^{13}\text{C}$  CP/MAS NMR) spectra were collected by a Bruker AVANCE III 400 NMR spectrometer. 2D Grazing incidence wide-angle X-ray scattering (GIWAXS) data were collected at 1W1A endstation, Beijing Synchrotron Radiation Facility ( $\lambda = 1.5496 \text{ \AA}$ ), using a MarCCD (mar345) with around 438 mm from the samples to CCD.

### Data availability

The data that support the findings of this study are available in the paper and its supplementary information files, or available from the corresponding author upon request. The fingerprint data that support the findings of this study are available from FVC2002, <http://bias.csr.unibo.it/fvc2002>.

### Code availability

The code (FingerPrint Matching: A simple approach) for fingerprint analysis associated with the current submission is available at <https://github.com/alilou63/fingerprint>, (Created by Vahid K. Alilou).

### References

- Derbel, N. & Kanoun, O. *Advanced Methods for Human Biometrics Ch* (pp. 1–2. Springer, Cham, 2021).
- Faulds, H. Poroscopy: the scrutiny of sweat-pores for identification. *Nature* **91**, 635–636 (1913).
- Memon, S. A., Manivannan, N. & Balachandran, W. Active pore detection for liveness in fingerprint identification system. In: *2011 19th Telecommunications Forum (TELFOR) Proceedings of Papers* (2011).
- Johnson, P. & Schuckers, S. Fingerprint pore characteristics for liveness detection. In: *2014 International Conference of the Biometrics Special Interest Group (BIOSIG)* (2014).
- Marasco, E. & Ross, A. A survey on antispoofing schemes for fingerprint recognition systems. *ACM Comput. Surv.* **47**, 1–36 (2015).
- Agarwal, R., Jalal, A. S. & Arya, K. V. A review on presentation attack detection system for fake fingerprint. *Mod. Phys. Lett. B* **34**, 2030001 (2020).
- Ding, B. et al. Subcutaneous sweat pore estimation from optical coherence tomography. *IET Image Process.* **15**, 3267–3280 (2021).
- Yuan, C., Sun, X. & Lv, R. Fingerprint liveness detection based on multi-scale LPQ and PCA. *China Commun.* **13**, 60–65 (2016).
- Lu, M.-Y., Chen, Z.-Q. & Sheng, W.-G. A pore-based method for fingerprint liveness detection. In: *2015 International Conference on Computer Science and Applications* (2015).
- Côté Adrien, P. et al. Porous, crystalline, covalent organic frameworks. *Science* **310**, 1166–1170 (2005).
- Ding, S. Y. & Wang, W. Covalent organic frameworks (COFs): from design to applications. *Chem. Soc. Rev.* **42**, 548–568 (2013).
- Medina, D. D. et al. Directional charge-carrier transport in oriented benzodithiophene covalent organic framework thin films. *ACS Nano* **11**, 2706–2713 (2017).
- Lohse, M. S. & Bein, T. Covalent organic frameworks: structures, synthesis, and applications. *Adv. Funct. Mater.* **28**, 1705553 (2018).
- Ma, T. et al. Single-crystal x-ray diffraction structures of covalent organic frameworks. *Science* **361**, 48–52 (2018).
- Guan, X. et al. Chemically stable polyarylether-based covalent organic frameworks. *Nat. Chem.* **11**, 587–594 (2019).
- Zhang, W. et al. Reconstructed covalent organic frameworks. *Nature* **604**, 72–79 (2022).
- Auras, F. et al. Synchronized offset stacking: a concept for growing large-domain and highly crystalline 2D covalent organic frameworks. *J. Am. Chem. Soc.* **138**, 16703–16710 (2016).
- Wang, Z., Zhang, S., Chen, Y., Zhang, Z. & Ma, S. Covalent organic frameworks for separation applications. *Chem. Soc. Rev.* **49**, 708–735 (2020).
- Huang, N., Chen, X., Krishna, R. & Jiang, D. Two-dimensional covalent organic frameworks for carbon dioxide capture through channel-wall functionalization. *Angew. Chem. Int. Ed.* **54**, 2986–2990 (2015).
- Zeng, Y., Zou, R. & Zhao, Y. Covalent Organic Frameworks for CO<sub>2</sub> Capture. *Adv. Mater.* **28**, 2855–2873 (2016).
- Fu, Y. et al. Zwitterionic covalent organic frameworks: attractive porous host for gas separation and anhydrous proton conduction. *ACS Nano* **15**, 19743–19755 (2021).
- Xu, H., Gao, J. & Jiang, D. Stable, crystalline, porous, covalent organic frameworks as a platform for chiral organocatalysts. *Nat. Chem.* **7**, 905–912 (2015).
- Kaczmarek, A. M. et al. Developing luminescent ratiometric thermometers based on a covalent organic framework (COF). *Angew. Chem. Int. Ed.* **59**, 1932–1940 (2020).
- Wang, S. et al. Programming covalent organic frameworks for photocatalysis: investigation of chemical and structural variations. *Matter* **2**, 416–427 (2020).
- Liu, X. et al. Recent advances in covalent organic frameworks (COFs) as a smart sensing material. *Chem. Soc. Rev.* **48**, 5266–5302 (2019).
- Ding, S. Y. et al. Thioether-based fluorescent covalent organic framework for selective detection and facile removal of mercury(II). *J. Am. Chem. Soc.* **138**, 3031–3037 (2016).
- Mal, A. et al. Supramolecular reassembly of self-exfoliated ionic covalent organic nanosheets for label-free detection of double-stranded DNA. *Angew. Chem. Int. Ed.* **57**, 8443–8447 (2018).
- Yusran, Y., Fang, Q. & Valtchev, V. Electroactive covalent organic frameworks: design, synthesis, and applications. *Adv. Mater.* **32**, e2002038 (2020).
- Vitaku, E. et al. Phenazine-based covalent organic framework cathode materials with high energy and power densities. *J. Am. Chem. Soc.* **142**, 16–20 (2020).
- Luo, R. et al. Intraregular charge transfer regulated electrochemiluminescence of donor-acceptor covalent organic frameworks. *Nat. Commun.* **12**, 6808 (2021).
- Song, Y.-W. et al. Covalent organic frameworks construct precise lithiophilic sites for uniform lithium deposition. *Matter* **4**, 253–264 (2021).
- DeBlase, C. R. et al. Rapid and efficient redox processes within 2D covalent organic framework thin films. *ACS Nano* **9**, 3178–3183 (2015).

33. Peng, P. et al. In situ charge exfoliated soluble covalent organic framework directly used for Zn-air flow battery. *ACS Nano* **13**, 878–884 (2019).
34. Ascherl, L. et al. Solvatochromic covalent organic frameworks. *Nat. Commun.* **9**, 3802 (2018).
35. Das, P., Chakraborty, G., Tyagi, S. & Mandal, S. K. Design of fluorescent and robust covalent organic framework host matrices for illuminating mechanistic insight into solvatochromic decoding. *ACS Appl. Mater. Interfaces* **12**, 52527–52537 (2020).
36. Jhulki, S. et al. Humidity sensing through reversible isomerization of a covalent organic framework. *J. Am. Chem. Soc.* **142**, 783–791 (2020).
37. Chen, L. et al. Covalent organic framework functionalized with 8-hydroxyquinoline as a dual-mode fluorescent and colorimetric pH sensor. *ACS Appl. Mater. Interfaces* **10**, 15364–15368 (2018).
38. Ascherl, L. et al. Perylene-based covalent organic frameworks for acid vapor sensing. *J. Am. Chem. Soc.* **141**, 15693–15699 (2019).
39. Gilmanova, L. et al. Chemically stable carbazole-based imine covalent organic frameworks with acidochromic response for humidity control applications. *J. Am. Chem. Soc.* **143**, 18368–18373 (2021).
40. Hao, Q. et al. Oriented two-dimensional covalent organic framework films for near-infrared electrochromic application. *J. Am. Chem. Soc.* **141**, 19831–19838 (2019).
41. Yu, F. et al. Electrochromic two-dimensional covalent organic framework with a reversible dark-to-transparent switch. *Nat. Commun.* **11**, 5534 (2020).
42. Bessinger, D., Muggli, K., Beetz, M., Auras, F. & Bein, T. Fast-switching vis-IR electrochromic covalent organic frameworks. *J. Am. Chem. Soc.* **143**, 7351–7357 (2021).
43. Hao, Q. et al. A covalent organic framework film for three-state near-infrared electrochromism and a molecular logic gate. *Angew. Chem. Int. Ed.* **60**, 12498–12503 (2021).
44. Thommes, M. et al. Physisorption of gases, with special reference to the evaluation of surface area and pore size distribution (IUPAC Technical Report). *Pure Appl. Chem.* **87**, 1051–1069 (2015).
45. Csösz, É., Emri, G., Kalló, G., Tsaprilis, G. & Tózsér, J. Highly abundant defense proteins in human sweat as revealed by targeted proteomics and label-free quantification mass spectrometry. *J. Eur. Acad. Dermatol. Venereol.* **29**, 2024–2031 (2015).
46. Towns, J. K. Moisture content in proteins: its effects and measurement. *J. Chromatogr. A.* **705**, 115–127 (1995).
47. Girod, A., Ramotowski, R. & Weyermann, C. Composition of fingerprint residue: a qualitative and quantitative review. *Forensic Sci. Int.* **223**, 10–24 (2012).
48. Alilou, V. K. FingerPrint matching: a simple approach (<https://github.com/alilou63/fingerprint>), GitHub (2023).
49. FVC2002 is the Second International Competition for Fingerprint Verification Algorithms. The fingerprint database (DB1\_B.zip) was downloaded from the website of FVC2002 (<http://bias.csr.unibo.it/fvc2000/>) (2002).
50. Lee, J. et al. Hydrochromic conjugated polymers for human sweat pore mapping. *Nat. Commun.* **5**, 3736 (2014).
51. Pyo, M. et al. Sweat pore mapping using a fluorescein-polymer composite film for fingerprint analysis. *Chem. Commun.* **51**, 3177–3180 (2015).
52. Lou, Q. et al. Water-triggered luminescent “nano-bombs” based on supra-(carbon nanodots). *Adv. Mater.* **27**, 1389–1394 (2015).
53. Cheng, Y. et al. Multiscale humidity visualization by environmentally sensitive fluorescent molecular rotors. *Adv. Mater.* **29**, 1703900 (2017).
54. Cai, L. et al. Chemical visualization of sweat pores in fingerprints using GO-enhanced TOF-SIMS. *Anal. Chem.* **89**, 8372–8376 (2017).
55. Xu, L., Li, Y., Wu, S., Liu, X. & Su, B. Imaging latent fingerprints by electrochemiluminescence. *Angew. Chem. Int. Ed.* **51**, 8068–8072 (2012).
56. Shi, M. et al. Label-free physical and electrochemical imaging of latent fingerprints by water and SECM. *Electrochim. Acta* **350**, 136373 (2020).

## Acknowledgements

This work was supported by the National Natural Science Foundation of China (22005312) (Q.H.) and (62271136) (C.Z.), the Key Research and Development Program of Jiangsu Province (BE2021700) (H.L.), Science and Technology Development Program of Suzhou (SYG202117) (H.L.), the Fundamental Research Funds for the Central Universities (2242022R10127) (Q.H.). We gratefully acknowledge the support of 1W1A endstation at Beijing Synchrotron Radiation Facility, Institute of High Energy Physics, Chinese Academy of Sciences. We gratefully thank Bo Guan and Jiling Yue of ICCAS for their assistance with TEM. The computing results described in this paper were obtained on the China National Grid (<http://www.cnggrid.org/>)/China Scientific Computing Grid (<http://www.scgrid.cn>).

## Author contributions

Q.H., D.W., and H.L. conceived the research idea. Q.H., X.R.R., and Y.C. performed experiments. C.Z. and J.X. helped with the software analysis. Q.H. wrote the paper. Q.H. and X.R.R. contribute equally. All authors discussed the results, analyzed the data, and reviewed the manuscript.

## Competing interests

The authors declare no competing interests.

## Additional information

**Supplementary information** The online version contains supplementary material available at <https://doi.org/10.1038/s41467-023-36291-9>.

**Correspondence** and requests for materials should be addressed to Qing Hao, Dong Wang or Hong Liu.

**Peer review information** *Nature Communications* thanks the anonymous reviewers for their contribution to the peer review of this work.

**Reprints and permissions information** is available at <http://www.nature.com/reprints>

**Publisher's note** Springer Nature remains neutral with regard to jurisdictional claims in published maps and institutional affiliations.

**Open Access** This article is licensed under a Creative Commons Attribution 4.0 International License, which permits use, sharing, adaptation, distribution and reproduction in any medium or format, as long as you give appropriate credit to the original author(s) and the source, provide a link to the Creative Commons license, and indicate if changes were made. The images or other third party material in this article are included in the article's Creative Commons license, unless indicated otherwise in a credit line to the material. If material is not included in the article's Creative Commons license and your intended use is not permitted by statutory regulation or exceeds the permitted use, you will need to obtain permission directly from the copyright holder. To view a copy of this license, visit <http://creativecommons.org/licenses/by/4.0/>.

© The Author(s) 2023